Decay of Turbulence in the Upper Ocean following Sudden Isolation from Surface Forcing

W. D. SMYTH

College of Oceanography and Atmospheric Sciences, Oregon State University, Corvallis, Oregon

P. O. ZAVIALOV

Departamento de Física, Fundação Universidade do Rio Grande, Rio Grande, RS, Brazil

J. N. MOUM

College of Oceanography and Atmospheric Sciences, Oregon State University, Corvallis, Oregon

(Manuscript received 4 October 1995, in final form 10 October 1996)

ABSTRACT

Measurements of velocity, hydrography, surface meteorology, and microstructure were made through several squall events during a westerly wind burst that occurred in the Western Pacific warm pool in December 1992. Sustained wind forcing generated a weakly stratified turbulent surface layer that extended to the top of the main thermocline. Following each rain event, freshwater formed a statically stable layer in the upper 4–12 m. The subsequent evolution of the mixing profile was strongly depth-dependent. Turbulence increased dramatically in the fresh layer adjacent to the surface but *decreased* in the underlying layer. The factor by which turbulence decreased following a given squall was strongly correlated with the net rainfall. The observed timescale for the decay of the turbulence was about 0.7 buoyancy periods, similar to decay times observed near the surface after sunrise. However, these decay times are significantly larger than those estimated indirectly (as the ratio of dissipation rate to turbulent kinetic energy) from turbulent patches in the thermocline. To account for the discrepancy, the authors hypothesize that turbulence production continues to act during the observed decay process, partially counteracting the effect of dissipation.

1. Introduction

The decay of turbulence in the absence of sources has been a central topic in turbulence research for many decades. In the geophysical context, an understanding of the decay process is a crucial prerequisite for the proper interpretation of turbulence observations. In the stably stratified ocean, turbulence often occurs in patches that are relatively rare. Do these patches persist for a time much longer than the natural timescale of the stratification (N^{-1}, where N is the Brunt–Väisälä frequency), or do they decay more quickly once their driving force is gone? Gibson (e.g., 1982) presented the case for long source-free lives, while others (e.g., Caldwell 1983; Gregg 1987) have argued that, in the absence of an energy source, decay times are comparable to N^{-1}. The correct interpretation of turbulence measurements depends upon which view is taken. We have some idea of the distribution of turbulent patches from microstructure measurements in varied flow regimes. If the patches are long-lived, relatively few source events are required to account for the number of patches observed. This is the essence of the ''big bangs'' versus ''continuous creation'' debate presented by Caldwell (1983; also see Gibson 1987).

Since turbulent patches in the thermocline have both temporal and horizontal scales that are small relative to the typical spacing between measured profiles in currently practical sampling schemes, we must consider the observational record of a given patch to consist only of a single profile. Therefore a *direct* measure of the decay rate is not possible. Instead, the turbulent kinetic energy (TKE) characteristic of the patch, and its viscous dissipation rate ϵ, are estimated independently, and their ratio is used to infer the decay rate. We refer to this as an ''indirect'' estimate of the decay rate. Alternatively, one may estimate the temperature variance of the patch and the thermal dissipation rate, χ, and combine the two to obtain the timescale for diffusive smoothing of temperature gradients. Dillon (1982), Crawford (1986), and Moum (1996) have employed different approaches to

Corresponding author address: Dr. William D. Smyth, College of Oceanic and Atmospheric Sciences, Oregon State University, Oceanography Admin. Bldg. 104, Corvallis, OR 97331-5503.
E-mail: smyth@oce.orst.edu

arrive at a common conclusion: The timescales for both viscous dissipation and diffusive smoothing are significantly less than a buoyancy period ($2\pi/N$, where N is the Brunt–Väisälä frequency).

A ''direct'' measure of the turbulence decay rate requires observation of the temporal evolution of turbulence following the removal of sources. One source of relevant information is laboratory experiments. As noted by Gregg (1987), most of the information about the decay of stratified turbulence comes from measurements of grid wakes. But these measurements actually investigate spatial decay away from a source, not temporal decay following removal of a source (Rohr et al. 1988, for example). Further, because of the finite dimensions of laboratory tanks, the observed decay is far from complete, and the Reynolds number is small compared with geophysical values. Direct numerical simulations (e.g., Metais and Herring 1989) are a promising source of information, but simulations in parameter ranges typical of ocean turbulence require computational hardware on a scale that is only now becoming practical. Large-eddy simulation techniques provide an alternative numerical approach, which is now being applied in oceanographic contexts (e.g., Siegel and Domaradzki 1994; Skyllingstad et al. 1996).

A few specific geophysical observations offer alternative views of the decay process. For example, turbulence in the mixed layer tends to be homogeneous over horizontal distances larger than the sampling interval and therefore offers the possibility of measuring decay directly. Brainerd and Gregg (1993, hereafter BG93) have examined the diurnal restratification process that occurs following the reversal of the surface buoyancy flux at sunrise. In this case, however, the change in surface forcing is slow, complicating the interpretation of the observed decay.

We believe that we have observed a clearer example of the decay process in the upper ocean following rainfall. The abrupt onset of heavy rains associated with squalls causes the sudden appearance of a fresh stable layer at the sea surface (cf. Price 1979). This stable fluid tends to isolate the preexisting mixed layer from surface forcing. As a result, there is a rapid attenuation of turbulence below the stable layer. The primary purpose of this paper is to quantify the decay rate of subsurface turbulence using data obtained during several squalls that occurred in the western equatorial Pacific during the westerly windburst of December 1992 (Smyth et al. 1996a,b) and to compare the results with indirect estimates from thermocline patch data. Observational methods are described in section 2. In section 3, we discuss meteorological observations of the squalls. In section 4, we describe the response of the temperature and salinity profiles to squall passage. The response of the mixing profile is discussed in section 5, along with several possible models of the observed turbulence decay. The observed decay of turbulence following rainfall provides clues to the mechanisms via which the turbulence was generated; these issues are considered in section 6. In section 7, the results are synthesized to provide a consistent scenario for the generation and maintenance of turbulence prior to rainfall and for its subsequent decay.

2. Experimental details

The field data used in this study were obtained from the R/V *Moana Wave*, which was stationed at the center of the Intensive Flux Array during the Intensive Observation Period (fall/winter of 1992/93) of the Tropical Ocean Global Atmosphere (TOGA) Coupled Ocean–Atmosphere Response Experiment (COARE). During the period 20 December 1992–12 January 1993, *Moana Wave* steamed slowly around the Improved Meteorological Instrument (IMET) buoy, which was tethered at 1°45′S, 156°E. *Moana Wave*'s course was chosen to head into squall lines wherever practical and to remain within 8 km of the IMET mooring. Vertical profiling of temperature, conductivity, and velocity microstructure was carried out using the microstructure profiler CHAMELEON (Moum et al. 1995). Typical time intervals between successive profiles were 6–10 minutes. Simultaneously, shipboard measurements of meteorological parameters and solar irradiance were recorded. From these data, net surface heat fluxes were computed using version 2.0 of the COARE bulk flux algorithm (Fairall et al. 1996). Buoyancy fluxes were obtained using the methods of Dorrestein (1979). For the present analyses, TKE dissipation rates were obtained from velocity microstructure data as vertical averages over approximately 1 m, then interpolated to a 1-m grid using cubic splines. Microscale temperature, salinity, and density data have been averaged into 1-m bins. Horizontal currents were measured via a 150-kHz RDI shipboard acoustic Doppler current profiler (ADCP) with 8-m pulse length and 4-m bin width.

3. Surface signature of squalls

The term squall, or squall line, refers to a convective atmospheric structure that is organized in a linear fashion and is associated with a cold front, increased winds, and strong precipitation. Over the equatorial ocean, squall lines are common, accounting for up to 50% of annual rainfall (e.g., Zipser 1977). At the ocean surface, the passage of a squall is generally accompanied by

- a rapid increase in wind speed (up to 70 kt),
- a drop in air temperature ($\sim$5°C),
- heavy rainfall (rain rates as high as 500 mm/h have been reported) (Houze 1977).

Because of changes in wind speed and air temperature, the sensible heat flux from the ocean may increase by a factor of 4. The latent heat flux generally follows the same pattern. A typical squall line propagates with a speed of about 10 m s^{-1} (Houze 1977) and extends

TABLE 1. Summary of squall events. Columns 2 and 3 give the time (UTC) at which intensified surface forcing was first observed at our location. Local time (column 4) is ten hours later than UTC. The precipitation and wind stress (columns 5 and 6, respectively) values are averages taken over a one-hour period following squall onset. Columns 7 and 8 give the time and depth intervals over which turbulence decay has been quantified. Column 9 contains the root-mean-square difference between the measured value of $\log_{10}\epsilon$ and the value predicted on the basis of surface similarity scaling, within the decay layer, prior to the onset of each squall.

Event	Date UTC	Onset time (UTC)	Onset time (Local)	P (mm/h)	τ (N m^{-2})	Decay interval (UTC)	Depth range (m)	$\delta\epsilon_b$
1	20Dec92	1933	0533	33.2	0.22	2022–2135	25–40	0.26
2	21Dec92	0702	1702	24.5	0.14	0743–0955	15–30	0.32
3	21Dec92	1950	0550	9.8	0.16	1934–2052	15–30	0.11
4	24Dec92	0940	1940	36.0	0.16	1204–1410	15–30	0.30
5	24Dec92	2027	0627	8.5	0.20	2110–2230	15–25	0.32
6	26Dec92	0718	1718	4.7	0.14	0806–1021	15–30	0.13
7	27Dec92	0915	1915	4.8	0.03	1021–1221	15–30	0.19
8	27Dec92	1846	0446	17.8	0.02	1920–2138	15–30	0.17
9	28Dec92	1053	2053	28.5	0.14	1215–1424	15–30	0.41
10	29Dec92	1343	2343	11.5	0.01	1422–1648	15–30	0.11
11	03Jan93	1844	0444	10.0	0.08	1844–2034	15–30	0.29
12	04Jan93	0141	1141	5.7	0.04	0152–0314	15–30	0.09
13	04Jan93	1404	0004	8.0	0.07	1404–1556	15–30	0.32

for 25 km in the direction of propagation, so that a fixed point on the ocean surface experiences direct squall forcing for a period of order 1 hour. While atmospheric phenomena related to squalls are understood reasonably well (see Young et al. 1995, for a detailed look at squalls in the COARE region), the ocean's response to a squall is less well known.

At least 19 events that we identify as squalls passed over the ship during the observation period. Of these, 15 occurred during the westerly windburst of December 1992–January 1993 (Smyth et al. 1996a,b) when the upper ocean was relatively well mixed. Events occurring after the windburst will not be considered here since the upper ocean was strongly stratified during that period and the physics of mixing was correspondingly different. Of the remaining 15 events, we have eliminated two due to insufficient data and are therefore left with a sample of 13 events (Table 1). In order to examine the dependence of the ocean's response upon the details of the surface forcing, we have included in this sample several events for which either rainfall or wind was relatively light. It is likely that some of these events would not qualify as ''squalls,'' according to the precise usage of that term (e.g., Barnes and Seickman 1984). Nevertheless, we have retained the designation for simplicity.

While the squalls occupied less than 3% of the total time of our observations, they accounted for 46% of the rainfall and for about 8% of the wind energy available for mixing the ocean during the wind burst. A typical squall event coincided with the appearance of a layer of relatively cool, fresh, highly turbulent water in the upper few meters. The layer remained distinct from the underlying water for several hours after the squall had passed, during which time it spread to a depth of 10–30 m. In this paper, we are concerned primarily with the behavior of the water column directly *beneath* this layer. Here, mixing processes that were occurring as the squall arrived were strongly attenuated afterward. In addition to revealing an important aspect of the ocean's response to squalls, this observation allows us to deduce useful information about the mixing processes that occur in the near-surface regime.

4. Thermohaline response to squalls

Our dataset includes 13 squalls, which varied widely in terms of the magnitude and time-dependence of the associated air–sea fluxes. Our main conclusions are supported by statistical analyses involving all 13 squalls; the two events shown in Fig. 1 are presented as illustrative examples. The first event is an example of an exceptionally strong and well-defined squall; the second is probably more typical of the squalls encountered during the cruise. Each event generated strong fluxes of momentum, heat, and freshwater at the ocean surface (Figs. 1a–c). Surface cooling was due mainly to a combination of the sensible flux due to rain (rain temperature tended to be ~4°C cooler than SST; C. Fairall 1993, personal communication) and wind-enhanced latent cooling (also see Smyth et al. 1996b; Flament and Sawyer 1995). The first of these two squalls occurred near sunrise. It was intense and short-lived and was preceded and followed by periods of weak surface forcing. The second event passed our location in early evening and was weaker and less isolated. Before the second squall, surface fluxes of momentum and heat were moderate. Following the squall, surface forcing decreased dramatically for about an hour. Strong winds then resumed, accompanied by moderate rainfall, and persisted for several hours.

Due to persistent strong winds associated with the windburst, the ocean was generally well-mixed down to ~70 m, that is, the top of the main thermocline

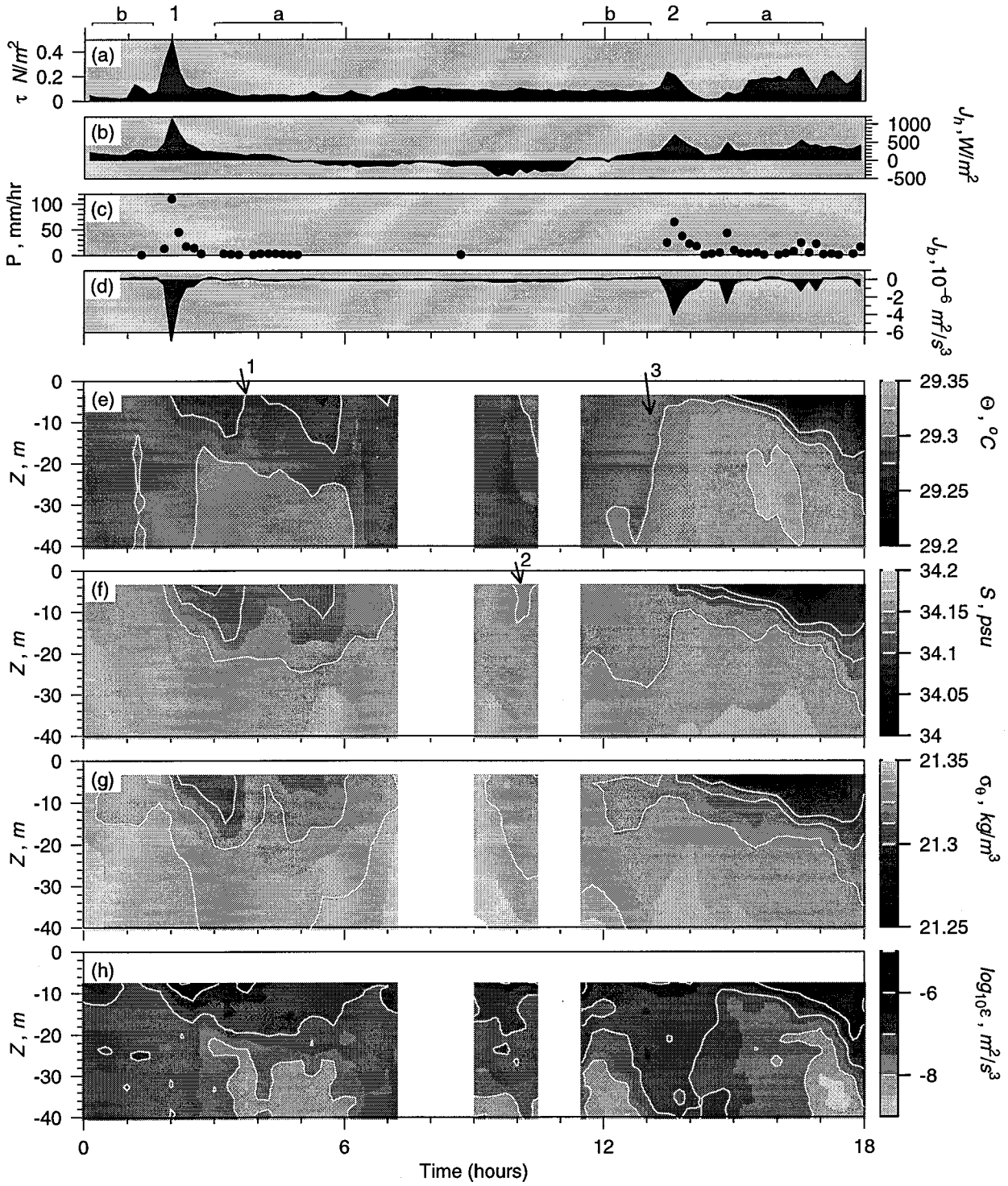

FIG. 1. Summary of meteorological and oceanographic measurements made over an 18-h period, beginning at 1811 UTC 20 December 1992 (Yearday 355.75), during which two squalls passed our location. (a) Squared magnitude of the surface wind stress; (b) net surface heat flux (including sensible flux due to rain); (c) rain rate (values less than 1 mm/h are omitted); (d) net surface buoyancy flux; (e) potential temperature; (f) salinity; (g) potential density; and (h) TKE dissipation rate. Meteorological variables are 10-min averages; subsurface quantities are obtained from profiles taken every 6–10 min, then gridded onto a 15-min grid. All fluxes are positive upward. Blank areas indicate intervals in which profiling was suspended due to other ship operations or instrument malfunctions. The time origin is 1800:00 UTC 20 December 1992. Time intervals indicated above (a) represent conditions obtaining before (''b'') and after (''a'') each of the two squalls and are employed in the statistical calculations described in section 5.

(Smyth et al. 1996b). Coincident with the passage of each squall, a distinct layer of cool, fresh water appeared at the surface, then spread through the upper 10–20 m over a period of a few hours (Figs. 1d,e). We refer to this layer as the *squall layer*. [Similar variability following rainfall has been observed by (Price) 1979.] The low temperature and low salinity of the squall layer affected density in opposite senses. In all cases examined here, the effect of reduced salinity was dominant, and the squall layer was therefore less dense than the underlying water (Fig. 1f). The resulting statically stable density stratification was of crucial importance in governing near-surface mixing.

A certain component of the variability we observed was due to lateral inhomogeneities being advected (in our reference frame) by the motion of the ship relative to near-surface currents. Interpretation of the ocean's response to the first squall is complicated by the fact that the *Moana Wave* moved out of the squall's wake about two hours after the squall passed, then changed direction (arrow 1 on Fig. 1) and steamed back into that region. Other observations that we attribute to the ship's motion relative to the ocean currents include the appearance of freshwater near the surface in the absence of rain (arrow 2), and the anomalous rise in subsurface temperatures coincident with the passage of the second squall (arrow 3). Given the relatively small spatial scale and short time period of the squalls, it is most probable that the ocean surface was scattered with cool, fresh puddles of various ages.

5. Decay of subsurface turbulence

Successive profiles of ϵ (Fig. 1g) taken following each of the squalls shown in Fig. 1 reveal two distinct changes. Within the squall layer, dissipation rates increased by an order of magnitude coincident with the increase in surface forcing. Below the squall layer, an equally dramatic *decrease* in ϵ is evident. The former change is not surprising; the visual appearance of the ocean surface during squalls featured large, breaking waves and frequent Langmuir cell activity, both of which are expected to produce vigorous mixing near the surface. The latter observation constitutes the main topic of the present paper. In section 5a, we present quantitative observations of the magnitude and generality of turbulence decay following squalls. In section 5b, we consider the observed decay to be due entirely to viscous dissipation of TKE. The results are consistent with those of BG93, but are inconsistent with indirect measures of decay. In section 5c, we attempt to resolve this discrepancy by assuming that TKE sources are present during the decay process.

a. Observations of turbulence decay

The effect of squall passage on ϵ is examined most readily in the case of squall number 1, because the squall layer penetrated more deeply than in any other case (presumably due to the exceptionally strong winds). As a result, profiler measurements of ϵ, which are contaminated near the surface by ship wake, were able to cover a substantial fraction of the squall layer. In Fig. 2, the evolution of the vertical structure of turbulence in the water column is illustrated in a sequence of time-averaged vertical profiles and compared to boundary layer similarity scaling. Although one cannot always expect similarity scaling to be representative (e.g., Anis and Moum 1995), it provides a useful guideline for comparison to the evolution of the turbulence before, during, and after the passage of the squall. Before the squall, $\epsilon(z)$ was consistent with similarity scaling (within a factor of 2), even though the stratification was not uniform (Fig. 2a). The immediate effect of the squall (which passed our location during the time period represented by Fig. 2b) was to attenuate ϵ relative to similarity scaling below 10-m depth. Simultaneously, freshwater input increased N^2 by a factor of 10 above 10 m. The downward diffusion of the squall layer is illustrated by the subsurface peaks in N^2 (also modulated by internal gravity waves), above which ϵ significantly exceeded similarity scaling and below which ϵ was significantly reduced (Figs. 2c,d). Finally, $\epsilon(z)$ appeared to revert to a similarity form approximately 3 hours following the first signs of the squall (Fig. 2e).

From the results illustrated in Fig. 2, we conclude that similarity scaling, which has sometimes been used to represent the dissipation rate profile (e.g., Dillon et al. 1981; Soloviev et al. 1988; Lombardo and Gregg 1989), provides an incomplete picture of the physical mechanisms driving turbulence in the wake of a squall. Enhanced mixing within the squall layer is presumably accounted for by wave breaking (e.g., Anis and Moum 1995), Langmuir cells (Weller and Price 1988), and enhanced near-surface shear. The attenuation of ϵ below the squall layer represents an important and instructive example of the decay of stratified turbulence following the removal of TKE sources. The physical mechanisms involved in this process will be discussed below. First, however, we quantify the rate and degree of turbulence attenuation and demonstrate that the damping of turbulence below the squall layer is a general feature of the squalls observed in this cruise.

Probability distribution functions for $log_{10}\epsilon$ in the depth range 15–30 m (i.e., below the squall layer), obtained during time intervals before and after squall number 2, were compared in order to quantify the suppression of turbulence (Fig. 3). Statistics of $\log_{10}\epsilon$ are considered, rather than those of ϵ itself, because the probability distribution of the former is less skewed than that of the latter (i.e., ϵ tends to follow a lognormal distribution; e.g., Davis 1996). The two distributions shown in Fig. 3 pass the Kolmogorov–Smirnov test for significantly different distributions, and the Student's t-test for significantly different means, at significance level 99% (i.e., the probability of the observed difference

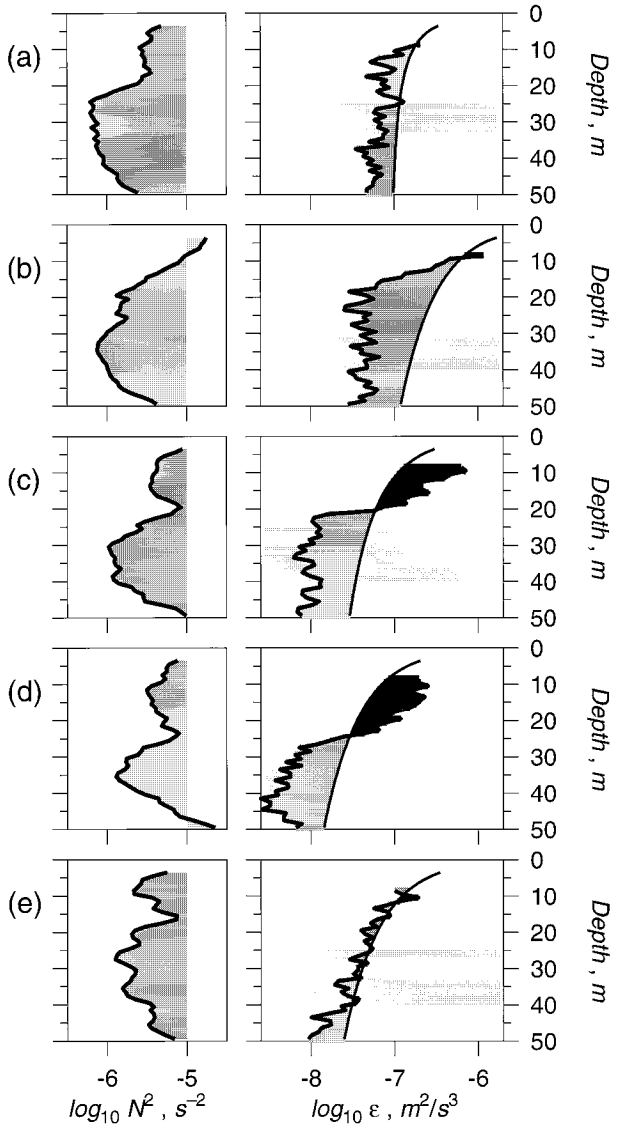

FIG. 2. Vertical profiles of N^2 (left-hand frame) and ϵ (right-hand frame), averaged over 10 consecutive profiles before (a; t = 0.2–1.6 h), during (b; t = 1.6–3.0 h) and after the passage of a squall (c, d, e: t = 3.0–4.4 h, t = 4.4–5.9 h, t = 5.9–7.3 h, respectively). The squall is number 1, illustrated in Fig. 1. For comparison, the depth-dependent effects of combined surface buoyancy flux and wind stress are approximated by boundary layer similarity scaling $\epsilon \sim u_*^3/\kappa z + 0.6J_b$, in which u_* is the friction velocity, $\kappa = 0.4$ is von Kármán's constant, and J_b is the surface buoyancy flux (Lombardo and Gregg 1989). The second term is included only when it is positive. Observed (theoretical) values are shown by the thick (thin) curve on the right-hand frame. Horizontal lines on the right-hand frames delineate the depth range over which the decay rate of ϵ was evaluated.

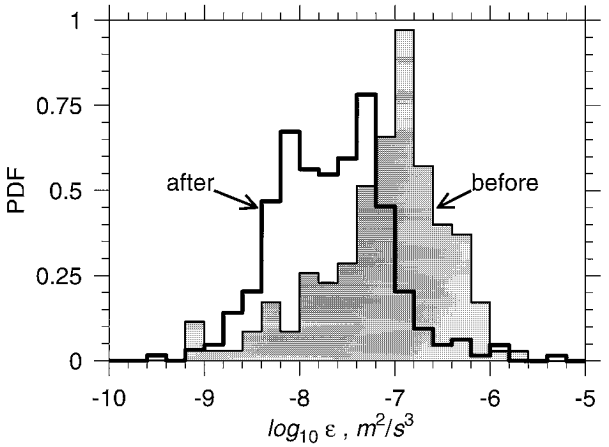

	before	after
Median	-7.00	-7.66
Mean	-7.12	-7.67
Standard Deviation	0.66	0.59
Standard Error in Mean	0.05	0.03

FIG. 3. Probability distribution functions for $log_{10}\epsilon$ in the depth range 15–30 m before and after squall number 2. The "before" ("after") case spans t = 11.5–13.0 h (t = 15.9–17.0 h). These intervals are intended to represent conditions prevailing when the squall arrived and during the ocean's recovery and were chosen subjectively on the basis of meteorological data only.

occurring by chance in two samples drawn from the same underlying distribution is less than 1%). Both the median and the geometric mean decreased by about a factor of 4. To test the generality of these results, 13 squalls were analyzed as described above. In 11 cases, ϵ decreased with significance level 99%. The decreases in the geometric mean ranged from a factor of 2 in the wake of a very weak squall to a factor of 27 following an exceptionally intense event.

b. Purely dissipative decay

The evolution of TKE under the sole influence of viscous dissipation is described by a reduced TKE equation:

$$\frac{\partial}{\partial t}\frac{3}{2}u^2 = -\epsilon, \tag{1}$$

in which u is a measure of the magnitude of the turbulent velocity fluctuations. A second equation connecting u and ϵ is the inviscid scale relation:

$$\epsilon = C_\epsilon u^3/l, \tag{2}$$

in which l is a length scale for energy-containing eddies. Equations (1) and (2) do not constitute a closed system since the evolution of l is unknown. Scaling considerations suggest that fluctuation amplitudes could exhibit a power-law decay with time (e.g., Tennekes and Lumley 1972); specifically, $\epsilon \sim t^{-2}$.

In contrast, our observations tend to suggest exponential decay (e.g., Fig. 4c). As BG93 have shown, exponential decay is predicted for turbulence in stably stratified flow when one assumes that the length scale of the energy-containing eddies is proportional to the Ozmidov scale, $L_O = (\epsilon/N^3)^{1/2}$, and neglects variability in N. Note that using $l = L_O$ in (2) yields $\epsilon = C_\epsilon u^2 N$,

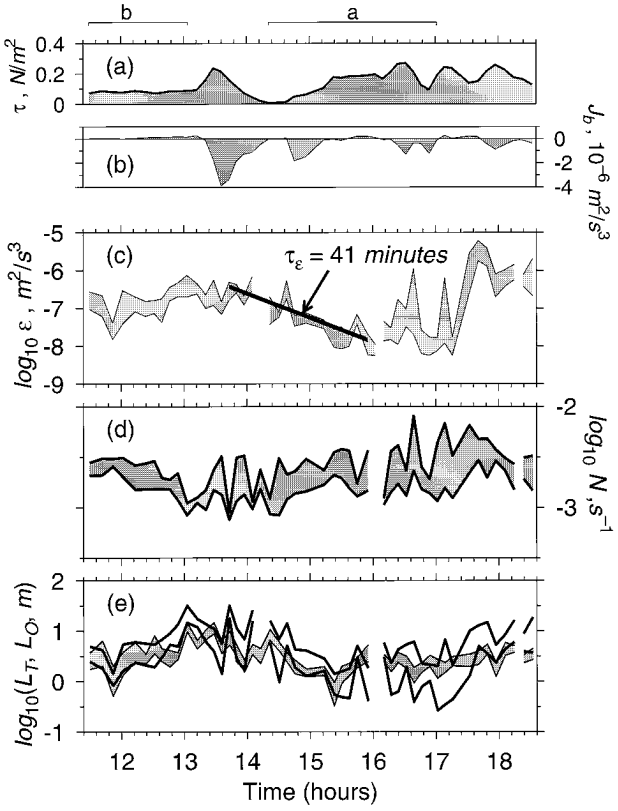

FIG. 4. Evolution of turbulence-related quantities before, during, and after squall number 2. As in Fig. 1, the labels ''b'' and ''a'' indicate the ''before'' and ''after'' intervals. (a) Wind stress magnitude; (b) surface buoyancy flux ($\times 10^6$); and (c) 95% confidence limits on depth-averaged ϵ in the depth range 15–30 m. The solid line represents a linear regression to depth-averaged ϵ between t = 13.7 h and t = 15.9 h. The slope yields an exponential decay time of τ_ϵ = 41 min, with 67% bootstrap (Efron and Tibshirani 1993) confidence limits of 35 and 48 min. (d) 95% confidence limits on depth-averaged N; (e) shaded strip: 95% confidence limits on Thorpe scale L_T. Solid curves: 95% confidence limits on Ozmidov scale L_O. Here L_T was computed from 5-cm-averaged profiles, then rms averaged over the given depth interval. Here L_O was computed as $\sqrt{\epsilon/N^3}$ using the depth-averaged values of ϵ and N shown in (c) and (d). The time origin is as in Fig. 1: 1800:00 UTC 20 December 1992.

the well-known scaling relation for stratified turbulence (e.g., Weinstock 1981). In applying (1) to the case of stratified turbulence, one should include an additional term, $-\Gamma\epsilon$, on the right-hand side, to account for conversion of TKE to potential energy. However, most studies indicate that the coefficient Γ is no larger than 0.2, so we neglect this term. Also neglected is the possibility of TKE loss via radiation of gravity waves. Following BG93, we substitute (2) into (1), using $l = aL_O$ (a is a constant proportionality), ignore the time evolution of N, and find that ϵ decays exponentially, that is, $\epsilon \sim \exp(-t/\tau_\epsilon)$. The ratio of the viscous decay time τ_ϵ to the buoyancy period $2\pi/N$ is a function of the constants a and C_ϵ:

$$\frac{\tau_\epsilon}{2\pi/N} = \frac{3}{4\pi}\left(\frac{a}{C_\epsilon}\right)^{2/3}. \tag{3}$$

Equation (3) is equivalent to BG93's Eq. (17) when one substitutes their value 0.84 for the constant a. [Note that BG93 phrased their results in terms of the constant C, which results from using the velocity scale $q = \sqrt{3}u$ in place of u in (2) and which is equal to $C_\epsilon/3^{3/2}$.] In what follows, we will employ (3) to obtain an estimate of C_ϵ. First, we discuss the validity of certain assumptions that were made in its derivation.

We begin with the assumption that the effect of the time evolution of N is negligible. The possible importance of restratification in modulating turbulence decay led BG93 to adopt a model in which N^2 varies linearly with time [cf. their Eq. (18)]. In contrast, we have found the simpler model (3), in which N is regarded as constant, to be acceptable. In our observations of variability following squall passage, N was as likely to decrease as to increase (cf. Fig. 7a). The clearest example of restratification following squall passage occurred following event number 2 (Fig. 4d); even here, the change in N was small compared to the change in ϵ. The absence of consistent restratification following squall passage is not surprising. The time over which turbulence decays following a typical squall is much smaller than the time required for the morning restratification (2 h vs 6 h), so restratification processes have a shorter interval in which to operate. In addition, BG93 found that about 60% of morning restratification is due to the divergent radiative heat flux, which is negligible in the cloudy conditions that generally follow a squall, particularly at the depths considered here.

In addition to neglecting the time-dependence of N, we have assumed the proportionality relation $l = aL_O$. This proportionality has been observed in several investigations, including those of BG93. We investigate the validity of this assumption by using the Thorpe scale L_T (Thorpe 1977) as a surrogate for l. The approximate proportionality between L_T and L_O is clear in the example shown in Fig. 4e. In addition, L_T and L_O were computed over the time intervals that define the decay regime for each of the events observed (Fig. 5). The geometric mean ratio of the length scales was 1.1 $\pm$ 0.2 (the error estimate is a 95% confidence limit). This is remarkably consistent with the results obtained by both Dillon (1982) and Moum (1996; Fig. 3a) in observations of turbulent patches in the thermocline but is somewhat larger than the value employed by BG93, a = 0.84. This discrepancy may be the result of different averaging procedures. In any case, the discrepancy is of little consequence for the present purposes, and we adopt the value a = 1.0 in the calculations presented here.

In order to evaluate C_ϵ from (1), we have estimated the rate at which subsurface turbulence decayed following each squall passage via linear fits to depth-averaged

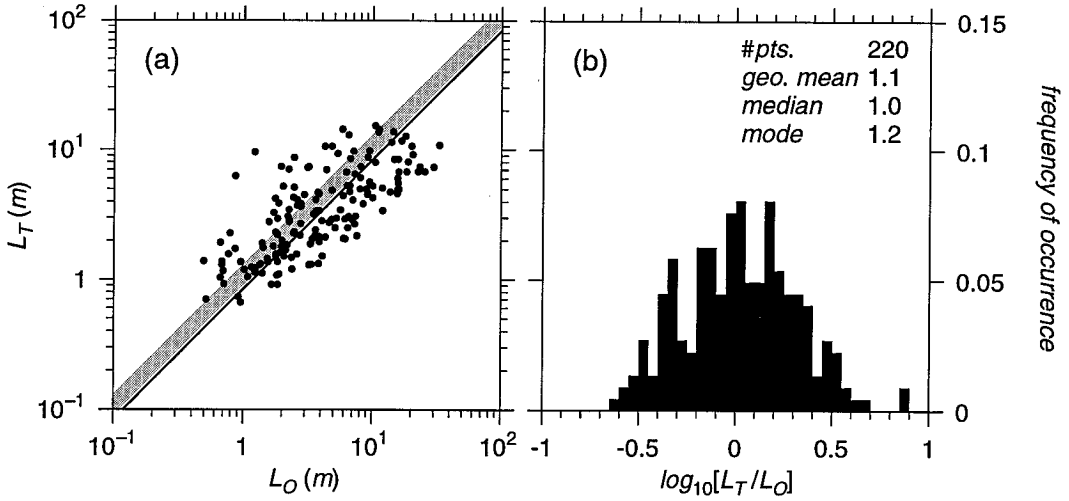

FIG. 5. (a) Thorpe ($\langle L_T \rangle$) and Ozmidov ($\langle L_O \rangle$) scales for the decay regime following each of the 13 rain events, computed profile-by-profile in the manner described in the caption to Fig. 4. The shaded strip indicates the 95% confidence limits on the geometric mean of the ratio, $a = L_T/L_O = 1.1 \pm 0.2$. The solid line corresponds to the value $a = 0.84$ employed by BG93. (b) Histogram of $\log_{10} a$.

$\log_{10}\epsilon$. In all cases, the fit was performed over a subjectively chosen interval of at least 10 profiles immediately following the onset of squall rains, during which ϵ decreased most rapidly (Table 1). In the case illustrated in Fig. 4, ϵ decreased with an *e*-folding time (τ_ϵ) of 40 min. Over all eleven events in which decay was observed, the average *e*-folding time was 47 ± 8 min. (The uncertainty estimate is twice the standard error in the mean, i.e., a 95% confidence limit if Gaussian statistics are assumed.) Extinction thus occurred on a temporal scale that is on the low end of the range of buoyancy periods observed, which varied between approximately 40 min (for $N^2 = 10^{-5}$ s^{-2}) and 2 h (for $N^2 = 10^{-6}$ s^{-2}) in this regime.

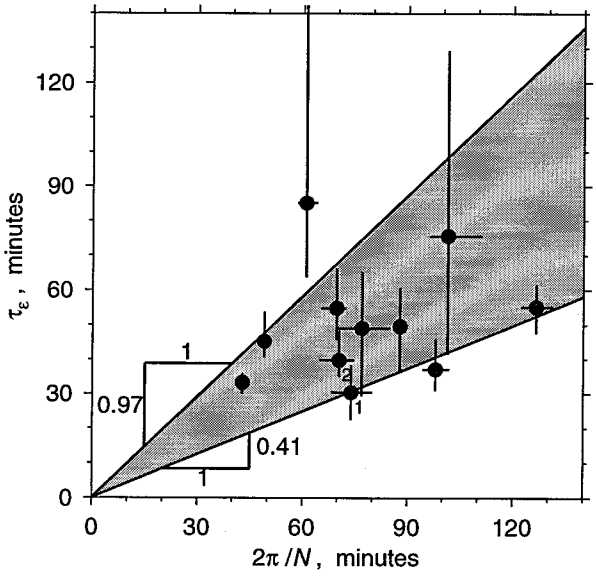

FIG. 6. Exponential decay time for depth-averaged dissipation rate versus buoyancy period for each of the 11 squalls during which turbulence was observed to decay. The error estimates on τ_ϵ and $2\pi/N$ are based on 95% bootstrap confidence limits. The range of slopes shown by the shaded area in (d) is twice the standard deviation of the 11 individual values. The subscripts "1" and "2" indicate the two squalls identified in Fig. 1; "2" is the squall shown in Fig. 4. For event 1, the depth interval for averaging was changed to 20–35 m since the squall layer was unusually deep in that case. The shallow slope indicated by the dotted line represents the theoretical value obtained using $C_\epsilon = 0.5$ in (5).

The average ratio of τ_ϵ to $2\pi/N$ was 0.69 with standard deviation 0.28. This direct measurement of the decay time scale for ϵ is significantly larger than the decay time of turbulent kinetic energy estimated indirectly from turbulent patches in the thermocline (Dillon 1982; Crawford 1986; Moum 1996). In contrast to the indirect estimates, we are unable to distinguish a clear correlation between the decay time and the local buoyancy period (Fig. 6). However, this is not surprising since our data covers a relatively small range of buoyancy periods. Our value 0.69 (0.41, 0.97) for the lhs of (3) results in an estimate 0.20 (0.12, 0.44) for C_ϵ. This is consistent with BG93's estimate $C_\epsilon \sim 0.2$ (or $C \sim 0.04$), despite the fact that the latter result was obtained using a generalization of (3), which accounted for restratification effects.

c. Decay in the presence of sources

Although the observations of turbulence decay quoted above are direct, the resulting estimates of C_ϵ are not, as they depend upon the validity of (1). Direct estimates of C_ϵ have been obtained by comparing independent and coincident measurements of ϵ, u^2, and l [cf. Eq. (2)] from stratified turbulence data in atmospheric boundary layers (Hunt et al. 1985) and the ocean's main ther-

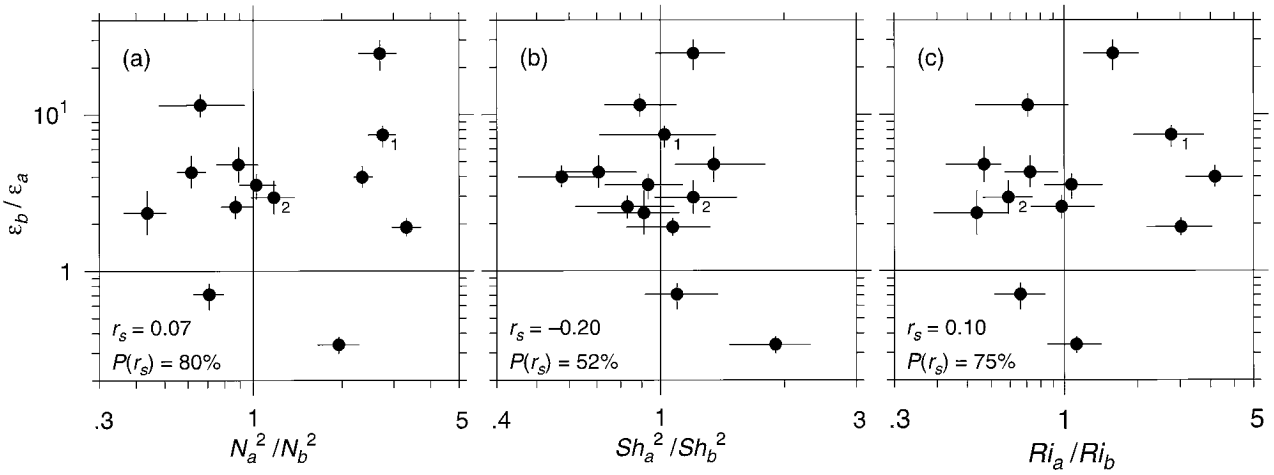

FIG. 7. (a) Ordinate is the ratio of the geometric means of ϵ before and after squall passage in the depth range 15–30 m (values greater than unity indicate suppression of turbulence). Abscissa is the ratio of geometric means of N^2, calculated using Thorpe-reordered profiles, after and before the squall (values greater than unity indicate increased stratification). As in Fig. 2 the ''before'' and ''after'' intervals comprised 10–20 profiles and were chosen on the basis of surface meteorology. The labels ''1'' and ''2'' indicate the cases identified in Fig. 1. For event ''1,'' the depth interval for averaging was changed to 20–35 m. Error bars indicate 95% confidence limits derived using the standard error in the mean before and after squall passage. (b) As above, but the abscissa is the ratio of squared vertical shear before and after the squall. For these calculations, the vertical derivatives in both shear and N^2 were computed as centered differences from data in 4-m vertical bins. Values greater than unity indicate increased vertical shear. (c) As above, but the abscissa is the ratio of the gradient Richardson number N^2/Sh^2, before and after the squall. Values greater than unity indicate increased Ri and would correlate with suppressed turbulence if the turbulence were driven by the local shear. Here r_S is the Spearman rank-order correlation coefficient (Press et al. 1992); $P(r_S)$ is the probability that r_S would exceed the given value for uncorrelated data. In each case shown here, that probability is 50% or higher. Our data thus provide no evidence for correlation between turbulence suppression and changes in ambient stratification, shear, or Richardson number. In this figure, all quantities have been calculated using data in 4-m vertical bins for consistency with the ADCP velocities.

mocline (Moum 1996). These direct estimates indicate C_ϵ to be in the range 0.4–0.6, greater by at least a factor of 2 than the indirect estimate determined above and by BG93 using (1). Still higher values ($C_\epsilon \sim$ 2–5) have been obtained by Peters et al. (1995) from analyses of thermocline patches, and by Kaimal and Haugen (1967), Kaimal (1973), and Wamser and Muller (1977) using atmospheric data. One may also estimate $C_\epsilon \sim O(1)$ on theoretical grounds (Weinstock 1981). Integrating the Kolmogorov spectrum (e.g., Tennekes and Lumley 1972) to estimate TKE, and taking the inviscid limit, one finds

$$\frac{3}{2}u^2 = \int_{l^{-1}}^{\infty} c_K \epsilon^{2/3} k^{-5/3}\, dk = \frac{3}{2} c_K (\epsilon l)^{2/3},$$

with the Kolmogorov constant $c_K \approx 1.5$. Rearranging, we recover (2) with $C_\epsilon = 0.54$. Estimates of C_ϵ thus fall roughly within an order-of-magnitude interval centered on unity. Values estimated indirectly from the observed decay of near-surface ocean turbulence (BG93 and the present paper) lie at the low end of that range. In what follows, we suggest a physical explanation for these relatively low values of C_ϵ.

Suppose other processes besides dissipation contributed to the evolution of TKE—could this account for the discrepancy in estimates of C_ϵ? To assess this possibility, we replace (1) with a revised TKE equation in which TKE sources (of unspecified origin) are included. To preserve exponential decay, we write the additional term as a fixed fraction, s, of the dissipation rate:

$$\frac{\partial}{\partial t}\frac{3}{2}u^2 = -\epsilon(1 - s). \tag{4}$$

To solve (4), we once again use (2) with $l = aL_O$, and C_ϵ, a, and N constants. With these substitutions, we obtain

$$\frac{\tau_\epsilon}{2\pi/N} = \frac{3}{4\pi(1 - s)}\left(\frac{a}{C_\epsilon}\right)^{2/3}. \tag{5}$$

Note that (3) is a special case of (5) with $s = 0$. The estimate of C_ϵ derived from (5) is very sensitive to the value of s, particularly since C_ϵ appears raised to a power less than one. Determination of C_ϵ from (3) is therefore dubious, unless sources are known to be absent.

How large must the ''source'' strength s be if our measurements of τ_ϵ are to be consistent with $C_\epsilon \sim O(1)$? If we take our direct estimate of

$$\frac{\tau_\epsilon}{2\pi/N} = 0.7,$$

the theoretical estimate $C_\epsilon = 0.54$ and $a = 1.0$, (5) yields $s \approx 0.5$. (This result is not very sensitive to the value used for C_ϵ: to obtain $C_\epsilon = 1.0$, one requires $s = 0.6$.) This implies that, if these direct estimates of C_ϵ are correct, the observed turbulence is decaying in the pres-

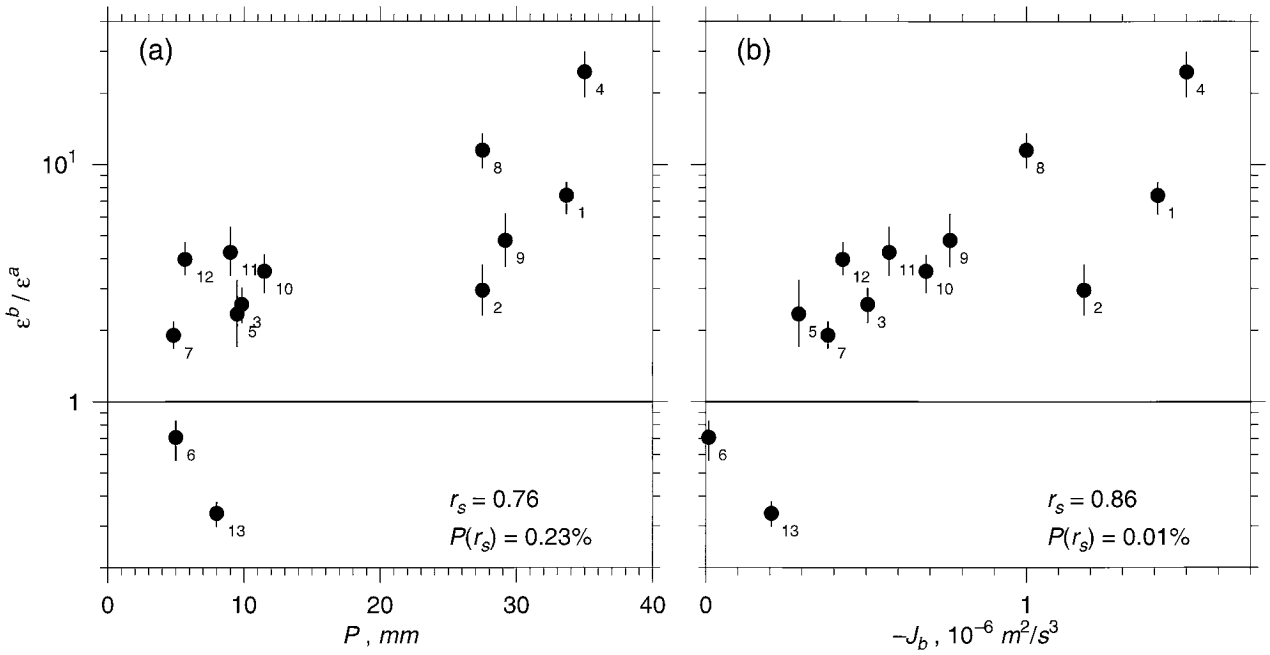

FIG. 8. (a) Abscissa is the total precipitation during squall passage. Ordinate is the ratio of the geometric means of ϵ before and after squall passage in the depth range 15–30 m (values greater than unity indicate suppression of turbulence). Error bars indicate 95% confidence limits derived using the standard error in the mean of $\log_{10}\epsilon$ before and after squall passage. (b) Abscissa is minus the average surface buoyancy flux during the event. Positive values indicate a stabilizing buoyancy flux. Large values of r_s confirm a strong correlation of turbulence suppression with rainfall and a stronger correlation with buoyancy flux. Each point is labeled with its event number (cf. Table 1).

ence of additional sources of TKE whose total magnitude is a substantial fraction (~50%) of the rate of TKE dissipation. We emphasize that TKE production does not continue unabated in this scenario; rather, its strength decays exponentially in proportion to ϵ.

We can also use (5) to obtain a revised estimate of the turbulence decay rate in the absence of sources by setting $s = 0$ and using $C_\epsilon = 0.54$ and $a = 1.0$. The result is $\tau_\epsilon = 0.36 \times (2\pi/N)$. This estimate is within the range of the indirect estimates of τ_ϵ obtained by Dillon (1982), Crawford (1986), and Moum (1996).

6. Implications for turbulence generation

The observed suppression of subsurface turbulence furnishes clues about the manner by which the turbulence was originally generated. Gradient Richardson numbers in the upper few tens of meters tended to be significantly less than 1/4 (e.g., Smyth et al. 1996a). One might suppose, then, that turbulence in this region was either driven locally by the instability of the mean current or maintained by Reynolds stress shear production. If this were true, the presence of the squall layer would have had to act to reduce the mean shear, and/or to increase N^2, in order to suppress turbulence. However, statistical tests fail to detect any consistent modulation of N^2, shear, or Ri associated with squalls (Fig. 7). While the geometric means of these quantities often changed significantly during the passage of a squall, each of the mean quantities was as likely to decrease as to increase. Furthermore, there is no evident correlation between the degree of turbulence reduction and the magnitude of the change in N^2, shear, or Ri. This suggests that turbulence decay was not due to a weakening of local production mechanisms. If this interpretation is correct, it follows that preexisting turbulence was maintained, at least in part, by some mechanism other than local production, and it was a change in this alternative mechanism that caused the observed decay.

We hypothesize that the alternative mechanism for local TKE maintenance was a downward flux of surface-generated turbulence. Prior to squall passage, weak stratification allowed surface-generated turbulence to be readily distributed over the upper few tens of meters, possibly as a result of advection by convective plumes, Langmuir cells (Weller and Price 1988), downwind rolls (Soloviev 1990), or orbital motions associated with surface waves (Anis and Moum 1995). Prior to squall onset, dissipation profiles in the decay layer tended to follow surface-layer similarity scaling to within a factor of 2. (The median of the rms discrepancy in $\log\epsilon$, shown in the rightmost column of Table 1, is 0.26, which corresponds to a factor of 1.8 difference in ϵ.) This suggests that at least a significant fraction of ambient turbulence was driven by wind and buoyancy forcing. With the onset of heavy precipitation, however, near-surface stability characteristics changed dramatically. The base of the squall layer was characterized by intense static sta-

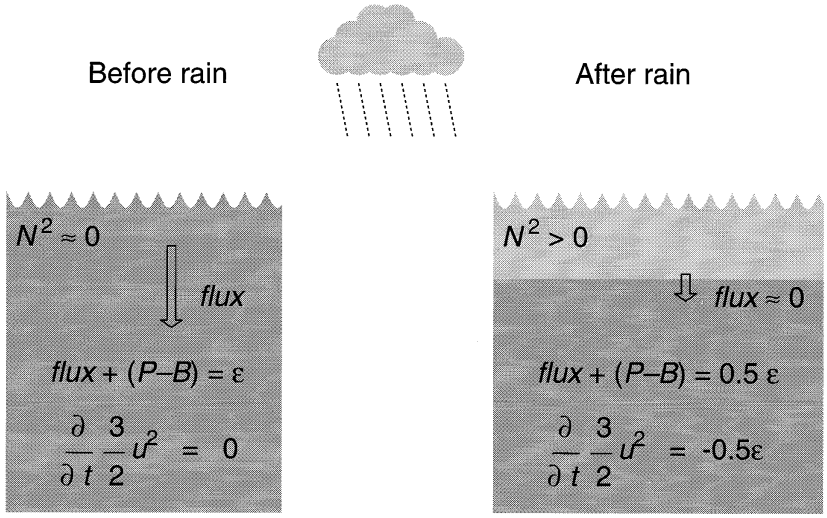

FIG. 9. Schematic representation of a scenario for turbulence decay consistent with present observations and with the value $C_\epsilon = 0.5$, which has been obtained previously (e.g., Moum 1996). Before the rain, TKE is maintained by a combination of local production (shear production P and buoyancy production $-B$) and the flux of TKE from the surface. Once the near-surface region has been stably stratified by freshwater input (this process corresponds to the creation of the squall layer, represented by light shading in the right-hand frame), the vertical TKE flux is substantially reduced, leading to a decay of turbulence. This decay process is in turn slowed by the continued action of local production mechanisms.

bility due to salt stratification. This stable stratification acted to inhibit downward transport of turbulence, thereby concentrating surface-generated turbulence within the squall layer. With the flux of turbulence from the surface thus suppressed, turbulence levels in the region below the squall layer decayed. The hypothesis just described is consistent with the absence of measurable correlation between turbulence suppression and changes in background shear and stratification (Fig. 7). Its validity is further supported by a positive correlation between turbulence suppression and the net precipitation during a given squall (Fig. 8a). The latter correlation also indicates that observed squall layers formed only a partial barrier to the downward transport of turbulence. Presumably, the increase in turbulence suppression with rainfall saturates at some point, so that the flux of TKE from the surface is completely arrested, and additional rainfall has no further effect. However, such asymptotic behavior is not evident in Fig. 8a, leading us to suggest that the hypothesized saturation level was not attained in any of the events we observed.

Of the events that lie away from the general trend of decay versus precipitation, several appear to have occurred at times when subsurface turbulence was already evolving rapidly due to the diurnal cycle of surface forcing. In particular, the two events during which ϵ was observed to *increase* both occurred during the early evening development of the nocturnal mixed layer. When the influence of the diurnal cycle is taken into account by using the total buoyancy flux as the independent variable instead of rainfall (Fig. 8b), the correspondence with turbulence decay is visibly improved. We have also tested for correlation of turbulence decay with wind speed and with the changes in buoyancy flux and wind speed during the squall. In each case, we were unable to detect any correlation.

The mechanism that we suspect caused reduced mixing below the squall layer has much in common with the ''barrier'' effect described by Lukas and Lindstrom (1991). In that scenario, the vertical heat flux is suppressed by stable salt stratification in a ''barrier layer.'' While an examination of heat fluxes in the wake of a squall is beyond the scope of the present work, we have seen that the vertical flux of TKE is suppressed by salt stratification in an analogous manner. Here, the squall layer plays the role of a barrier layer, insulating the underlying water from the flux of TKE originating at the surface.

7. Summary and discussion

Statistical analysis of 13 individual rain events indicates that attenuation of subsurface mixing is a consistent feature of the oceanic mixing profile in the wake of heavy rainfall. We suggest that this is due to a reduction of the flux of surface-generated TKE below the squall layer due to the stable stratification created by freshwater input. In support of this hypothesis, we have noted that the degree of turbulence attenuation is well correlated with net rainfall. The correlation improves when the influence of the diurnal cycle is considered by replacing rainfall by the total buoyancy flux. How-

ever, the suppression of TKE flux is incomplete, as is evidenced by changes in the response of the flow below the squall layer associated with incremental changes in surface forcing. We have found that, following isolation of the preexisting mixed layer from the surface by the rainfall-induced stratification, TKE dissipation rates below the squall layer decay with *e*-folding times significantly less than the local buoyancy period. The resulting value of the constant C_ϵ; that is, $C_\epsilon = 0.2$ agrees with the estimate obtained by BG93 during morning restratification. This value is smaller than direct measurements and theoretical estimates (e.g., Moum 1996 and references therein), though not by as much as the results of BG93 might suggest due to the distinction between C and C_ϵ [cf. (3) and accompanying discussion]. The discrepancy may be explained as a result of the incomplete removal of TKE sources during the decay process.

We have seen evidence that the observed decay of ϵ is due to a cessation (or at least a substantial reduction) of the downward flux of surface-generated TKE (cf. section 6). On the other hand, we have seen evidence that a significant source of TKE is present during the decay phase (section 5c). This source could be the remaining TKE flux from the surface. However, the nearly exponential decay of ϵ (e.g., Fig. 4) suggests that the source decays in proportion to ϵ, which the flux from the surface is unlikely to do. An alternative possibility is that local production mechanisms operate during the decay phase at a rate smaller than, but comparable to, the dissipation rate. The production terms are, like ϵ, proportional to quadratic combinations of turbulent fluctuations, and could therefore decay in proportion to ϵ even if there were no change in background conditions.

The suggested scenario is illustrated schematically in Fig. 9. Prior to squall passage, local production reinforces the flux from the surface to maintain TKE at a roughly constant level. Following the rainfall, the region beneath the squall layer is isolated from the surface TKE flux, but local production continues as Reynolds stresses associated with the remaining turbulence interact with the ambient shear. The result is that turbulence decays, but much more slowly than it would if sources were removed entirely (as might be the case in an unsheared environment). This scenario allows $C_\epsilon \sim O(1)$ to be reconciled with observed decay rates—both directly measured decay in the near-surface region due to reversals of the surface buoyancy flux (BG93 and the present study) and dissipative decay inferred from thermocline patch data (Crawford 1986; Moum 1996).

Acknowledgments. We are grateful to Chris Fairall and George Young for sharing their high quality surface meteorological data with us and to Doug Caldwell and Hemantha Wijesekera for helpful comments. This work was supported by the National Science Foundation (OCE 9110552).

REFERENCES

Anis, A., and J. N. Moum, 1995: Surface wave–turbulence interactions: Scaling $\epsilon(z)$ near the sea surface. *J. Phys. Oceanogr.,* **25,** 2025–2045.

Barnes, G. M., and K. Seickman, 1984: The environment of fast- and slow-moving tropical mesoscale convective cloud lines. *Mon. Wea. Rev.,* **112,** 1782–1794.

Brainerd, K. E., and M. C. Gregg, 1993: Diurnal restratification and turbulence in the ocean surface mixed layer. 2. Modeling. *J. Geophys. Res.,* **98,** 22 657–22 664.

Caldwell, D. R., 1983: Oceanic turbulence: Big bangs or continuous creation? *J. Geophys. Res.,* **88,** 7543–7550.

Crawford, W. R., 1986: A comparison of length scale and decay times of turbulence in stably stratified flows. *J. Phys. Oceanogr.,* **16,** 1847–1854.

Davis, R. E., 1996: Sampling turbulent dissipation. *J. Phys. Oceanogr.,* **26,** 341–358.

Dillon, T. M., 1982: Vertical overturns: A comparison of Thorpe and Ozmidov scales. *J. Geophys. Res.,* **87,** 541–549.

——, J. G. Richman, C. G. Hansen, and M. D. Pearson, 1981: Near surface turbulence measurements in a lake. *Nature,* **290,** 390–392.

Dorrestein, R., 1979: On the vertical buoyancy flux below the sea surface as induced by atmospheric factors. *J. Phys. Oceanogr.,* **9,** 229–231.

Efron, B., and R. J. Tibshirani, 1993: *An Introduction to the Bootstrap.* Chapman and Hall, 436 pp.

Fairall, C., E. F. Bradley, D. P. Rogers, J. B. Edson, and G. S. Young, 1996: The TOGA COARE bulk flux algorithm. *J. Geophys. Res.,* **101,** 3747–3764.

Flament, P., and M. Sawyer, 1995: Observations of the effect of rain temperature on the surface heat flux in the intertropical convergence zone. *J. Phys. Oceanogr.,* **25,** 413–419.

Gibson, C. H., 1982: Alternative interpretations for microstructure patches in the thermocline. *J. Phys. Oceanogr.,* **12,** 374–383.

——, 1987: Oceanic turbulence: Big bangs and continuous creation. *J. Physiochem. Hydrodyn.,* **8,** 1–22.

Gregg, M. C., 1987: Diapycnal mixing in the thermocline: A review. *J. Geophys. Res.,* **92,** 5249–5286.

Houze, R. A., Jr., 1977: Structure and dynamics of a tropical squall-line system. *Mon. Wea. Rev.,* **105,** 1540–1567.

Hunt, J. C. R., J. C. Kaimal, and J. E. Gaynor, 1985: Some observations of turbulence structure in stable layers. *Quart. J. Roy. Meteor. Soc.,* **111,** 793–815.

Kaimal, J. C., 1973: Turbulence spectra, length scales and structure parameters in the stable surface layer. *Bound.-Layer Meteor.,* **4,** 289–309.

——, and D. A. Haugen, 1967: Characteristics of vertical velocity fluctuations observed on a 430m tower. *Quart. J. Roy. Meteor. Soc.,* **93,** 305–317.

Lombardo, C. P., and M. C. Gregg, 1989: Similarity scaling of viscous and thermal dissipation in a convecting surface boundary layer. *J. Geophys. Res.,* **94** (C5), 6273–6284.

Lukas, R., and E. Lindstrom, 1991: The mixed layer of the western equatorial Pacific Ocean. *J. Geophys. Res.,* **96,** 3343–3357.

Metais, O., and J. R. Herring, 1989: Numerical simulations of freely evolving turbulence in stably stratified fluid. *J. Fluid Mech.,* **202,** 117–148.

Moum, J. N., 1996: Energy-containing scales of stratified turbulence. *J. Geophys. Res.,* **101** (C6), 14 095–14 110.

——, M. C. Gregg, R. C. Lien, and M. E. Carr, 1995: Comparison of turbulent kinetic energy dissipation rates from two ocean microstructure profilers. *J. Atmos. Oceanic Technol.,* **12,** 346–366.

Peters, H., M. C. Gregg, and T. B. Sanford, 1995: Detail and scaling of turbulent overturns in the Pacific Equatorial Undercurrent. *J. Geophys. Res.,* **100,** 18 349–18 368.

Press, W. H., S. A. Teulosky, W. T. Vetterling, and B. P. Flannerty, 1992: *Numerical Recipes in Fortran.* 2d ed. Cambridge University Press, 936 pp.

Price, J. F., 1979: Observations of a rain-formed mixed layer. *J. Phys. Oceanogr.*, **9,** 643–649.

Rohr, J. J., E. C. Itsweire, K. N. Helland, and C. W. van Atta, 1988: Growth and decay of turbulence in a stably stratified shear flow. *J. Fluid Mech.*, **195,** 77–111.

Siegel, D. A., and J. A. Domaradzki, 1994: Large-eddy simulation of decaying, stably stratified turbulence. *J. Phys. Oceanogr.*, **24,** 2353–2386.

Skyllingstad, E. D., T. Paluskiewicz, D. W. Denbo, and W. D. Smyth, 1996: Nonlinear vertical mixing processes in the ocean: Modeling and parameterization. *Physica D*, **98,** 574–593.

Smyth, W. D., D. Hebert, and J. N. Moum, 1996a: Local ocean response to a multiphase westerly windburst. Part 1: The dynamic response. *J. Geophys. Res.*, **101,** (C10), 22 495–22 512.

——, ——, and ——, 1996b: Local ocean response to a multiphase westerly windburst. Part 2: Thermal and freshwater responses. *J. Geophys. Res.*, **101,** (C10), 22 513–22 533.

Soloviev, A. V., 1990: Coherent structures at the ocean surface in convectively unstable conditions. *Nature*, **364,** 157–160.

——, N. V. Vershinsky, and V. A. Bezverchnii, 1988: Small-scale turbulence measurements in the thin surface layer of the ocean. *Deep-Sea Res.*, **35,** 1859–1874.

Tennekes, H., and J. L. Lumley, 1972: *A First Course In Turbulence*. The MIT Press, 300 pp.

Thorpe, S. A., 1977: Turbulence and mixing in a Scottish Loch. *Philos. Trans. Roy. Soc. London, Ser. A*, **286,** 125–181.

Wamser, C., and H. Muller, 1977: On the spectral scale of wind fluctuations within and above the surface layer. *Quart. J. Roy. Meteor. Soc.*, **103,** 721–730.

Weinstock, J., 1981: Energy dissipation rates of turbulence in the stable free atmosphere. *J. Atmos. Sci.*, **38,** 880–883.

Weller, R. A., and J. F. Price, 1988: Langmuir circulation in the oceanic mixed layer. *Deep-Sea Res.*, **35,** 711–747.

Young, G. S., S. M. Perugini, and C. W. Fairall, 1995: Convective wakes in the equatorial western Pacific during TOGA. *Mon. Wea. Rev.*, **123,** 110–123.

Zipser, E. J., 1977: Mesoscale and convective-scale downdrafts as distinct components of squall-line structure. *Mon. Wea. Rev.*, **105,** 1568–1589.